Sensitivity of Upwelling Radiance in Nimbus 6 HIRS Channels to Multilayered Clouds

ROBERT G. FEDDES AND KUO-NAN LIOU

Department of Meteorology, University of Utah, Salt Lake City, Utah 84112

An infrared radiative transfer model is developed that can simulate the effects of clouds on satellite upwelling radiances at the top of the atmosphere for a range of satellite scan angles. The model allows the calculations of the upwelling radiance for single layers of middle or high clouds and for multilayered clouds. Sensitivity analyses are carried out for the upwelling radiance in the presence of clouds in the Nimbus 6 high-resolution infrared sounder (HIRS) channels. Computational results show that thick cirrus cloud reduces the upwelling radiance most in both single and multicloud cases. Thin cirrus and thin middle clouds show a greater decrease in the upwelling radiance in comparison with thin cirrus and thick middle clouds in CO_2 channels where the weighting functions peak in or above the thin middle cloud. More variability is noted between window and water vapor channel upwelling radiances than is present in the CO_2 channels. Shortwave CO_2 channels are further shown to have a greater sensitivity to changes in cloud scenes than longwave CO_2 channels. We show that the effect of the atmospheric temperature profile is minimized by dividing the clear column radiance into the cloudy radiance. By utilizing the actual HIRS data a case study for the determination of the cloud thickness based on the theoretical sensitivity analyses has been carried out. When infrared and visible cloud pictures from the NOAA 4 satellite are compared, the case study shows some promise of cloud parameter determination using the combination of infrared channels.

1. INTRODUCTION

The structure and the composition of clouds obtained from passive remote sensing from satellites on a routine basis have been extremely limited. Many of the methods utilized are based strictly on statistical analysis of the observed data. The first attempts to recover cloud information from the broadband visible channel on the ITOS and NOAA series of satellites was in the form of cloud cover. These are represented by publications such as *Miller and Feddes* [1971]. With the addition of the broadband infrared channel on the NOAA series, analysis was accomplished on both channels at the same time. A further use of the broadband visible channel to infer statistically cloud thickness from the visible channel was done by *Park et al.* [1974] and *Kaveney et al.* [1977].

The recovery of cloud parameters from satellites in partly cloudy atmospheres was first attempted by *Houghton and Hunt* [1971] in which they explored the inference of cirrus clouds from passive remote sensing. *Liou* [1974] described emission and transmission properties of cirrus clouds in the 10-μm window in conjunction with their remote sensing potential. *Bunting and Conover* [1976] proposed a simple means for estimation of vertical ice content of cirrus clouds by assuming exponential attenuation of the infrared (IR) radiation. *Chahine* [1974] presented a numerical procedure to derive vertical temperature profiles in cloudy atmospheres from two overlapping fields of view. *Taylor* [1974] described an approach employing sounding at two different zenith angles to determine temperature profiles in the presence of clouds. These last two studies removed the cloud effect rather than incorporating it into the transfer equation. Recently, *Liou* [1977] developed a retrieval technique for recovering the thickness and ice content of cirrus clouds employing four spectral regions in the 10-μm window.

The launch of the Nimbus 6 satellite made available data in an expanded number of IR channels and for the first time upwelling radiances in the microwave portion of the spectrum. These two sources of data have been used by *Smith and Woolf* [1976] to recover temperature and water vapor profiles and cloud parameters simultaneously. In this paper we describe results of the infrared transfer model for cloudy atmospheres in the channels of the Nimbus 6 high-resolution infrared sounder (HIRS). Sensitivities of single-layered and multilayered clouds on the satellite upwelling radiances are investigated. Section 2 of this paper describes the HIRS instrument and the characteristics of the channels utilized in the analysis. This section also describes the model atmosphere used to perform the calculations. Section 3 describes how the transfer program was developed and the methods used to generate the required input for the calculations. Section 4 is an analysis of the sensitivity of the upwelling radiance to the combination of different cloud thicknesses. In section 5 we describe a case study in which the actual HIRS data have been used for the determination of the cloud thickness based on the theoretical sensitivity analyses. Finally, section 6 gives some conclusions and additional research that could be carried out to make this method usable in the routine recovery of cloud information from HIRS-type satellite data.

2. CHARACTERISTICS OF HIRS CHANNELS AND MODEL ATMOSPHERE

The Nimbus 6 HIRS instrument is a third-generation infrared radiation sounder. This instrument is similar to the infrared temperature profile radiometer (ITPR) on the Nimbus 5 satellite. The instrument scans perpendicular to the satellite subtrack. There are 42 scan spots per scan line with a resolution of 23 km near nadir and 31 km at the extremes of the scan. The Nimbus 6 satellite was successfully launched in June 1975, and the HIRS instrument has short periods during which all channels were operating successfully. We obtained a sample of good data from W. L. Smith (private communication, 1976) that covers the period August 20–30, 1975, with a geographical coverage of 80°–150°W and 20°–50°N. These data will be used for comparison in work subsequent to the sensitivity analysis described here.

The HIRS instrument senses infrared radiation in 17 channels. These include seven channels in the 15-μm CO_2 band, five channels in the 4.3-μm CO_2 band, water vapor channels at 6.8

Paper number 7C0757.

TABLE 1. HIRS Channel Characteristics

Channel	ν, cm^{-1}	λ, μm	Principal Absorbers	Level of Maximum (Weighting Function, mbar)
1	668	15.0	CO_2	30
2	679	14.7	CO_2	60
3	690	14.4	CO_2	100
4	702	14.2	CO_2	250
5	716	14.0	CO_2	500
6	733	13.6	CO_2/H_2O	750
7	749	13.4	CO_2/H_2O	900
8	900	11.0	Window	Surface
9	1224	8.2	H_2O	900
10	1496	6.7	H_2O	400
11	2190	4.57	N_2O	950
12	2212	4.52	N_2O	850
13	2242	4.46	CO_2/N_2O	700
14	2275	4.40	CO_2/N_2O	600
15	2357	4.24	CO_2	5
16	2692	3.71	Window	Surface

and 8.3 μm, and three channels in windows at 11, 3.68, and 0.69 μm.

In this analysis, only those channels which peak below 100 mbar would be substantially affected by clouds; therefore this sensitivity analysis will include only those channels. The information compiled in Table 1 and Figure 1 is taken from *Smith et al.* [1975]. The table includes channel number, wavelength, wave number, principal absorbers, and the approximate peaks of the weighting function. Figure 1 is a plot of the weighting functions for the channels in Table 1. The peaks in this figure indicate the approximate locations in the troposphere from which their energies are derived.

The model atmosphere used in this analysis was the mid-latitude summer atmosphere described by *McClatchey et al.* [1971] and is portrayed in Figure 2. The left-hand side of this figure depicts temperature, mixing ratio, and pressure profiles as functions of height. Owing to the computational time and the actual HIRS data that we have obtained, we felt that the sensitivity analysis would be carried out on only the mid-latitude summer atmosphere. This atmosphere is also significant, since follow-on analysis will involve mid-latitude summer data.

The model atmosphere was divided in such a way that it would coincide with the pressure levels used in the clear column radiance program (CCR) developed by *Smith and Woolf* [1976] and supplied to us for our use. There are 40 pressure levels for the CCR program. The CCR utilizes predetermined transmission profiles, and then they are adjusted as a function of the atmospheric profile used. It includes contributions from all the major gases listed in Table 1. To utilize further this predetermined vertical structure and to facilitate the execution

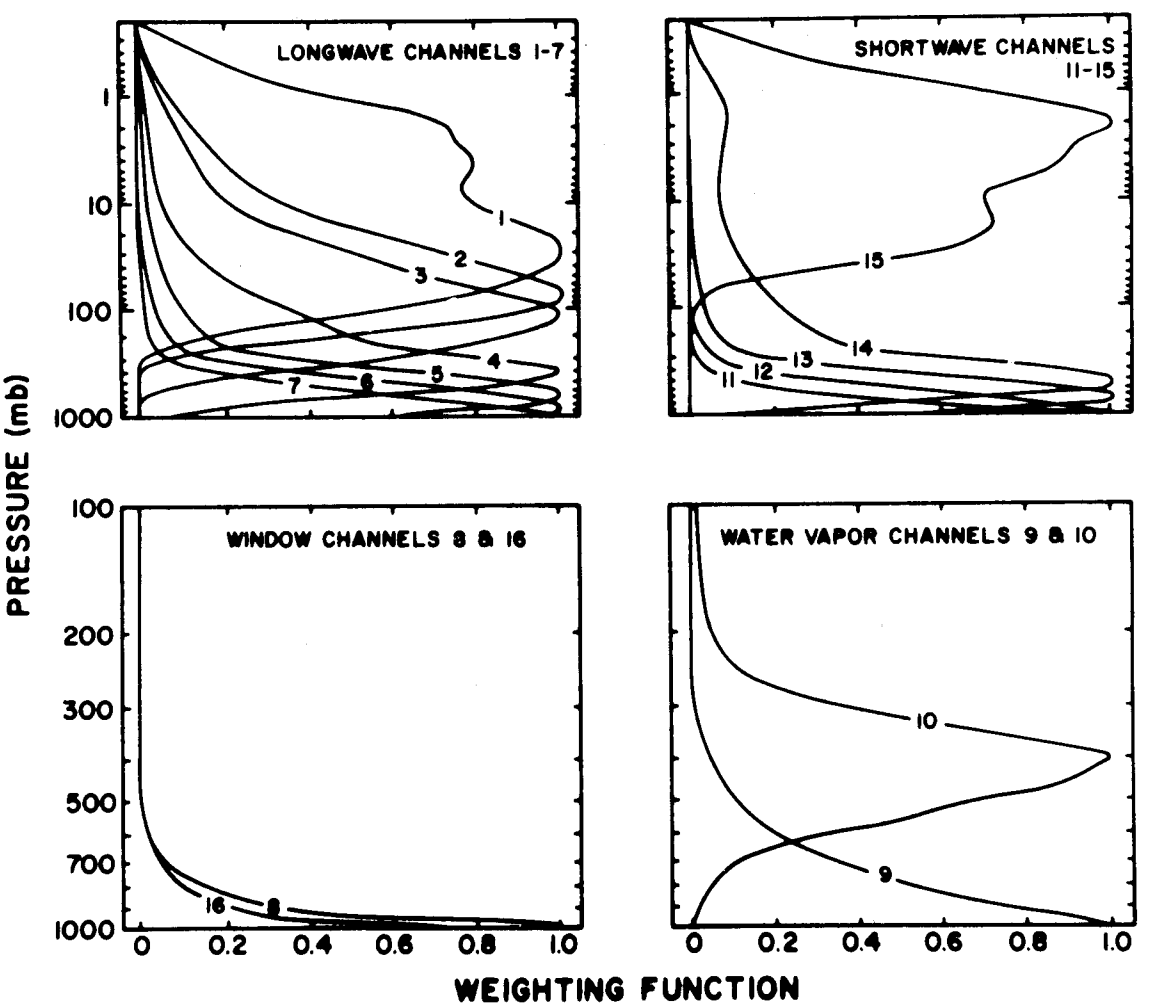

Fig. 1. The weighting functions of the HIRS channels.

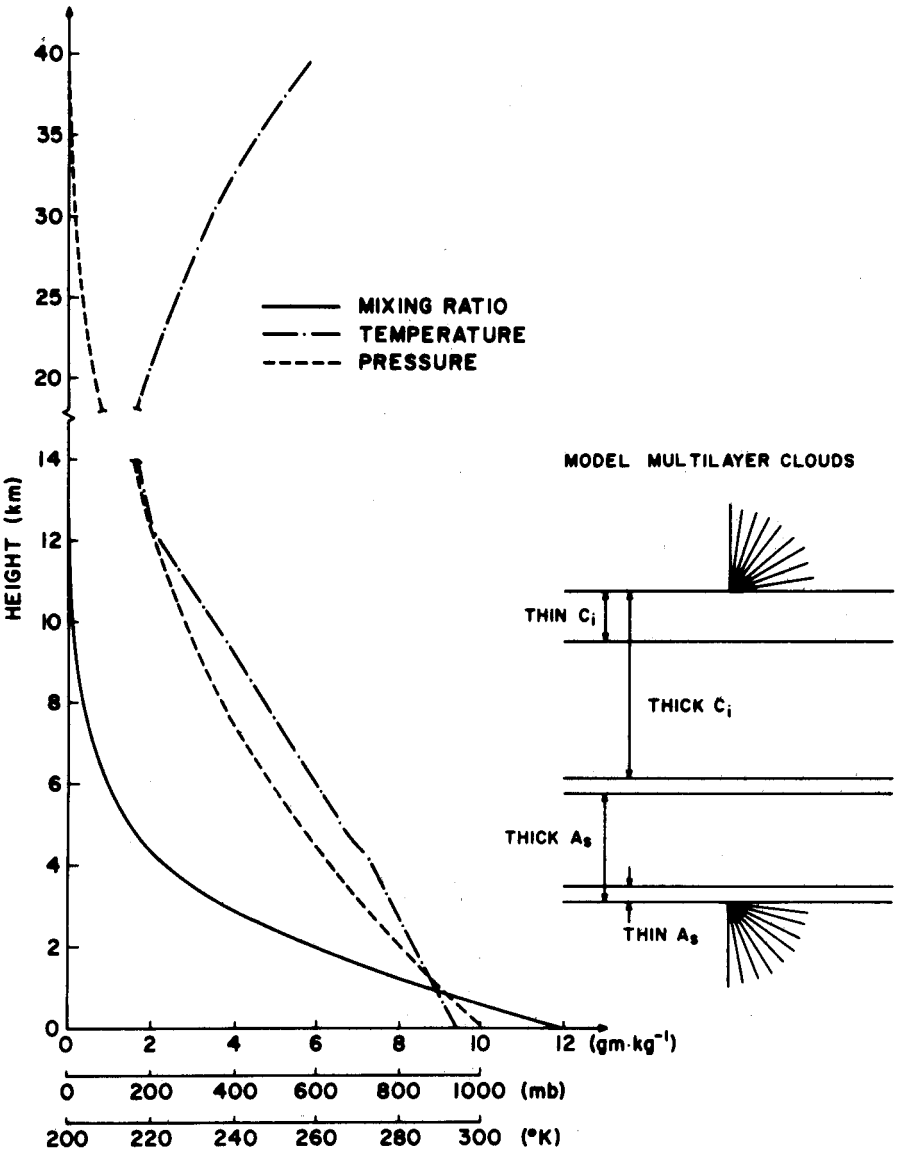

Fig. 2. Mid-latitude summer atmosphere from the surface to 40 km for temperature (in degrees Kelvin), pressure (in millibars), and water vapor mixing ratio (in grams per kilogram). The right-hand side shows the atmospheric location for thick and thin cirrus and middle cloud and the discrete angles used in the discrete ordinate method for radiative transfer.

of the cloud transfer program, the base of the middle cloud was fixed at 700 mbar, and the top of the high cloud was fixed at 250 mbar. The thicknesses of the high and middle clouds were allowed to vary from 1.26 to 4.12 km and from 0.35 to 2.68 km, respectively (right-hand side of Figure 2). These values represent realistic thickness variations for high and middle clouds in the atmosphere. Thus three distinct layers with changing thicknesses are formed. The infrared transfer program described below is developed to include all the possible combinations of thickness variations.

3. Description of the Infrared Transfer Program

This section describes (1) the generation of boundary conditions from CCR calculations, (2) gaseous contribution to the cloud transmissions, (3) the cloud optical properties, (4) the contribution above the cloud to the final upwelling radiance, and (5) cloud transfer calculation.

a. Boundary Conditions

The generation of the upper and lower boundary conditions for the transfer program utilized a CCR program provided by W. L. Smith (personal communication, 1976) that calculated CCR transmission values at all 40 pressure levels up to 0.1 mbar over the range of scan angles of the HIRS instrument. This program was modified to calculate transmission values at eight discrete ordinate angles of 8.35°, 19.17°, 30.05°, 40.94°, 51.84°, 62.74°, 73.64°, and 84.55° shown in the right-hand side of Figure 2 in conjunction with radiative transfer calculations involving clouds.

The upper boundary conditions were calculated directly by computing the CCR at each of the required discrete ordinate angles and then numerically integrating the equation for the upper boundary condition (downward radiances at the cloud top):

$$I_{\Delta\nu}^{\downarrow}(z_t; -\mu_i) = \int_{z_t}^{\infty} B_{\Delta\nu}[T(z)]dT_{\Delta\nu}(z, z_t; -\mu_i)$$

where $\Delta\nu$ denotes the spectral interval, z_t the cloud top height, μ_i the cosine of the discrete ordinate angle, $B_{\Delta\nu}$ the Planck function, T the temperature, and $T_{\Delta\nu}$ the transmittance for the

spectral band $\Delta\nu$. The upper boundary condition was calculated by summing the contribution of each layer above 250 mbar. The numerical values of the boundary conditions increase with increasing angle, which is physically correct, since the longer path lengths are involved at larger angles with respect to the satellite nadir angle or the cloud top zenith angle.

By utilizing the same output for the lower boundary condition (upward radiances at the cloud base) an adjustment had to be made in the transmission values below 700 mbar. This was required, since the transmission calculation from the satellite transmission function becomes very small below 700 mbar, especially for channels that peak high in the atmosphere. To adjust the satellite transmittances in reference to the top of the atmosphere relative to the base of the cloud, we evaluate the transmission function for the ith layer below the cloud by means of the relation $T_{\Delta\nu}{}^{ij} = 1 - |T_{\Delta\nu}{}^{i} - T_{\Delta\nu}{}^{j}|$, where $T_{\Delta\nu}{}^{ij}$ is the contribution from the adjacent layers below the cloud, j denotes the layer below the ith layer, and $T_{\Delta\nu}{}^{i}$ represents the satellite transmittance at the ith layer. This procedure was repeated for all levels down to the surface, and thus a transmission function relative to the base was produced. For channels that peak high in the troposphere (channels 4, 14, and 10) the transmission function was virtually zero below 700 mbar. Therefore it was assumed that there was no contribution from layers between the surface and the cloud base, and thus a constant upward radiance reaching the cloud base at each discrete angle was employed.

These transmittances were then calculated for all remaining channels, utilized in the analysis for a satellite scan angle of 0°. These vertical transmittances were then calculated for the discrete ordinate angles by using the equation

$$T_{\Delta\nu}(u/\mu) \approx \sum_{j=1}^{N} w_j \exp(-k_j u/\mu)$$

where u is the vertical path length, k_j is an equivalent absorption coefficient, w_j is the weight, and N is the total number of terms derived from the exponential fitting. By performing numerical integration on the equation for the lower boundary condition given by

$$I_{\Delta\nu}{}^{\uparrow}(z_b; \mu_i) = B_{\Delta\nu}(T_s)T_{\Delta\nu}(z_b, o; \mu_i) + \int_0^{z_b} B_{\Delta\nu}[T(z)]dT_{\Delta\nu}(z_b, z; \mu_i)$$

we obtain the upwelling radiance contribution reaching the cloud base from the surface and the atmosphere below, where z_b is the cloud base height. It should be noted that the lower boundary conditions at the discrete angles are relative to a zenith angle of 90°, which in effect increases the values of the upward radiances as the cloud limb is approached owing to the emission contribution from the atmosphere below the cloud.

b. *Gaseous Absorption in the Cloud Layers*

The contribution of the absorbing gases within the cloud layer in the transfer calculation was handled by an equation similar to that used to fit the lower boundary condition. This fitting utilized the approximation to the vertical transmittance given by

$$T_{\Delta\nu}(u) \simeq \sum_{j=1}^{N} w_j \exp(-k_j u)$$

where u is the vertical path length of the major absorber and, as in the lower boundary condition case, k_j is the equivalent absorption coefficient, w_j is the weight, and N denotes the total number of finite terms in the fitting of the transmissions. This equation is identical to the one used for the lower boundary condition except that the angular dependence is no longer necessary in the cloud layers. Note here that the amount of water vapor within ice and water clouds is estimated from the saturation condition over ice and water, whereas the amount of carbon dioxide within the clouds is assumed to be the same as that of the environment.

c. *Cloud Optical Properties*

The single scattering parameters for cirrus clouds and altostratus clouds were calculated by using Mie type scattering computations for the central wave-number in each band. The cirrus cloud was assumed to be entirely ice, and the altostratus cloud was assumed to be all water.

Calculation for the ice crystal parameters utilized a theoretical model developed by *Liou* [1972] which used ice cylinders randomly oriented in a horizontal plane. The major and minor axes of the cylinder used are 200 and 60 μm, respectively, with a concentration of 0.05 cm^{-3}. Table 2 lists the optical properties of the ice cylinders. The real and imaginary parts of the index of refraction are taken from the recent measurement by *Schaaf and Williams* [1973]. From Table 2 it is apparent that the real part of the index of refraction tends to increase with increasing wave number and the imaginary part decreases with increasing wave number. The single scattering albedo is largest in the window channels (channels 16 and 8), and the extinction cross section is greatest in the 15-μm band (channels 4–7).

The single scattering parameters for the water cloud utilized a drop size distribution developed by *Feddes and Smith* [1974]. This distribution is an exponential fitting of the best published

TABLE 2. Optical Properties of Cirrus and Altostratus Clouds

Channel	ν, cm^{-1}	Ice				Water			
		n_r	n_i	$\tilde{\omega}_0$	β_{ext}, km^{-1}	n_r	n_i	$\tilde{\omega}_0$	β_{ext}, km^{-1}
4	701.91	1.556	0.305	0.533	1.464	1.193	0.356	0.442	13.05
5	716.83	1.556	0.305	0.533	1.464	1.193	0.356	0.442	13.05
6	732.55	1.556	0.305	0.533	1.464	1.193	0.356	0.442	13.05
7	749.18	1.556	0.305	0.533	1.464	1.193	0.356	0.442	13.05
14	2274.63	1.299	0.0218	0.527	1.391	1.333	0.0128	0.719	13.82
13	2244.21	1.299	0.0218	0.527	1.391	1.333	0.0128	0.719	13.82
12	2211.97	1.299	0.0218	0.527	1.391	1.333	0.0128	0.719	13.82
11	2191.02	1.299	0.0218	0.527	1.391	1.333	0.0128	0.719	13.82
16	2691.20	1.392	0.007	0.625	1.360	1.372	0.00356	0.867	13.58
8	899.99	1.101	0.280	0.698	1.33	1.147	0.105	0.487	11.77
10	1508.29	1.316	0.057	0.51	1.326	1.332	0.035	0.619	14.69
9	1223.22	1.307	0.04	0.698	1.33	1.287	0.035	0.677	15.72

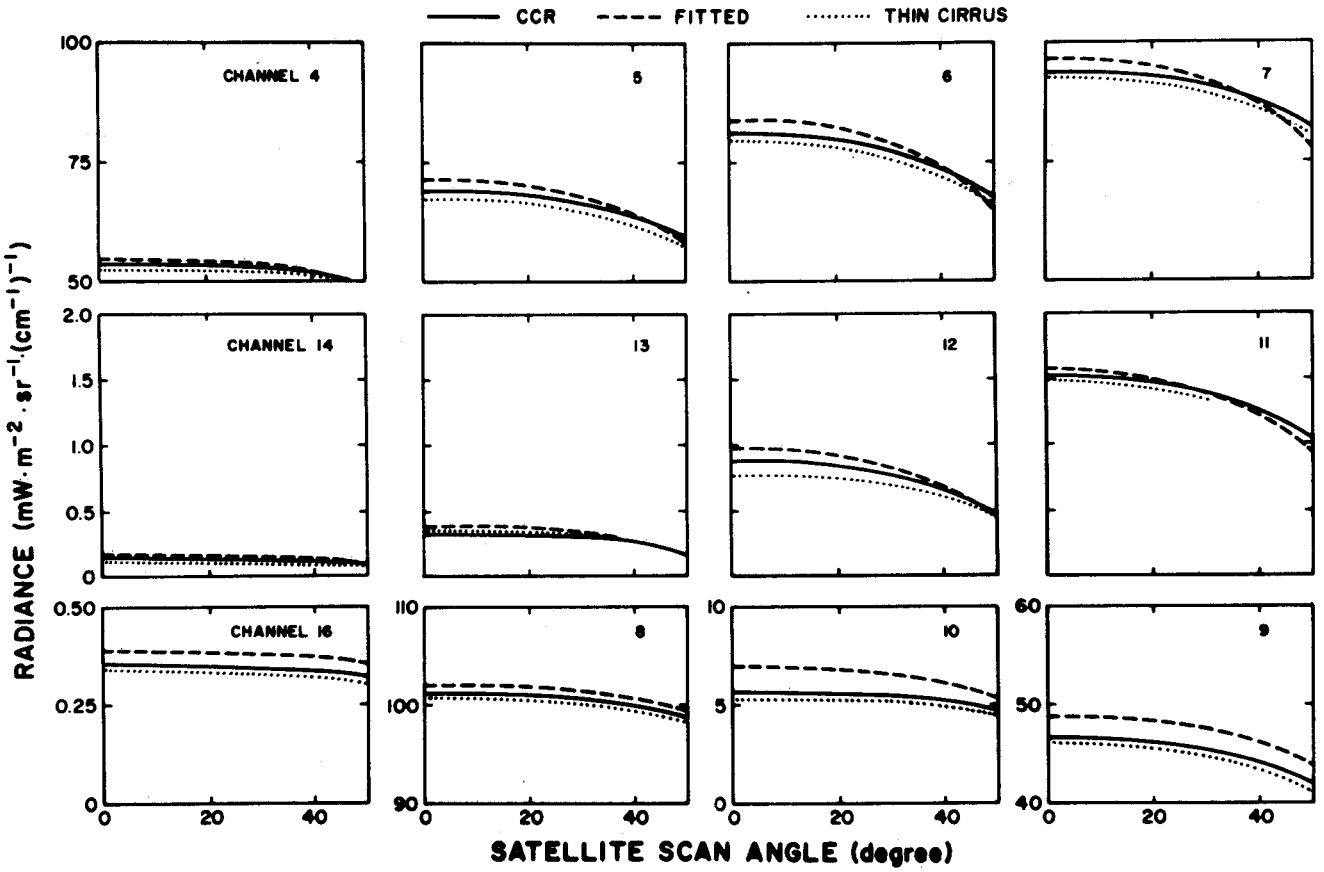

Fig. 3. Comparison of the clear column radiances (CCR) evaluated from the satellite transmittance (solid lines) with those obtained from the exponential fitting of the transmittance (dashed lines) and with radiances calculated from the spectral radiative transfer program assuming a thin cloud with a thickness of 0.01 km (dotted lines).

measurements taken from cloud physics literature. Although this fitting was done for 10 cloud types, only the altostratus cloud distribution is used. In the calculation of the single scattering parameters for altostratus clouds a liquid water content of 0.15 g m^{-3} was used. Table 2 also contains the optical properties of the water droplets. The real and imaginary parts of the index of refraction for each band were taken from *Hale and Querry* [1973]. From Table 2 it can be seen that the real part of the index of refraction generally increases with increasing wave number and the imaginary part decreases. The single scattering albedo is the largest, corresponding to the largest wave number, and the extinction cross section is the greatest in the water vapor bands (channels 9 and 10). Only one calculation was made for each of the CO_2 bands, since the real and imaginary parts of the index of refraction vary slowly.

d. *Contribution Above the Cloud*

To obtain the upwelling radiance at the top of the atmosphere, it is necessary to account for the contribution in the atmosphere above the cloud. This step is accomplished by executing the CCR program over a range of satellite scan angles larger than the extremes of the HIRS instrument scan (±36.9°). Because only one atmosphere is utilized, this calculation can be made once and for all. Since the top of the cirrus cloud is held constant throughout the calculation, the approximation introduced by using precalculated transmissions is constant for channels and cloud thicknesses. The transfer calculation assumes a plane parallel atmosphere. In this case the scan angle of the satellite is equal to the angle made by the satellite with the local zenith. When it is viewed from a satellite at scan angles greater than zero, the resolution of the instrument decreases with increasing scan angle. This decrease in resolution is due to the increase in the distance between the satellite and the sampling point and the curvature of the earth. To account for this difference due to the curvature of the earth, the CCR program uses the angle the earth's local zenith makes with the satellite, which is derived from the satellite scan angle. In this way the contribution to the final upwelling radiance from above the cloud top accounts for the curvature of the earth, and as a result the plane parallel assumption is minimized.

e. *Cloud Transfer Program*

Once the boundary conditions have been generated, the gaseous absorption in the clouds has been fitted, and the optical properties of the ice and water have been calculated, the cloud transfer program can now be utilized. The transfer calculations are based on the discrete ordinate solution to the radiative transfer equation developed by *Chandrasekhar* [1950]. This solution was used by *Liou* [1973] to solve the transfer equation in cloudy and hazy atmospheres.

Prior to the calculation of the data used in the sensitivity analysis, two tests were made. One test was to check the accuracy of the exponential fitting of the gaseous absorption in the clouds, and the second was to check the accuracy of the cloud transfer program applicable to the HIRS channels.

To test the fitting of the gaseous absorption, all three layers in the transfer calculation are assumed to be composed of

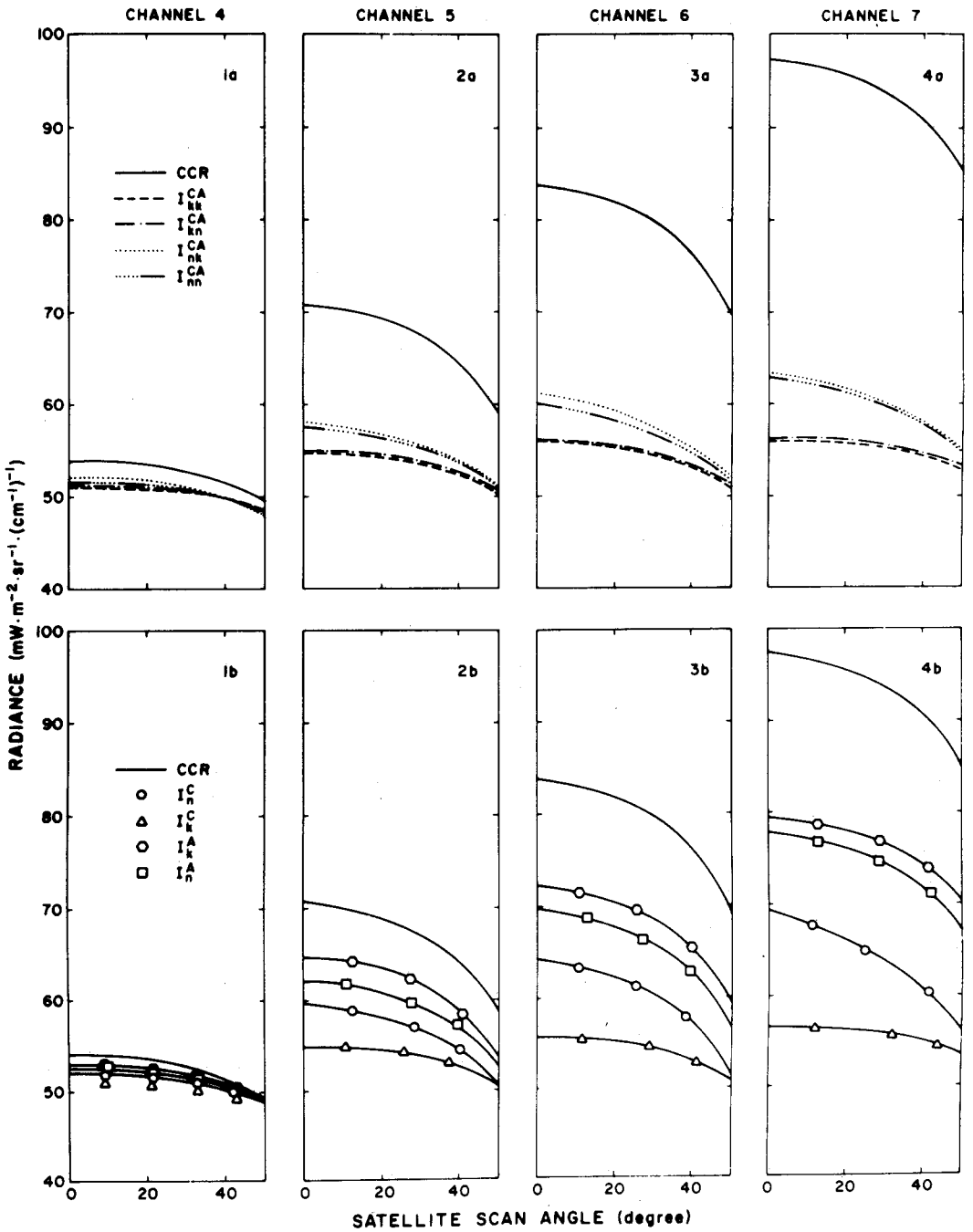

Fig. 4. Comparison of the upwelling radiance for cloudy atmospheres with CCR in longwave CO_2 channels. The upper panels are for multilayer combinations of thick and thin cirrus and middle cloud. The lower panels are for single layers of thick and thin cirrus and middle cloud.

gases only (Rayleigh layers). The resulting upwelling radiances from this calculation were compared to the upwelling radiances calculated with the clear column radiance program. A plot of this comparison is given in Figure 3. An examination of the figure indicates that all the channels have slightly higher upwelling radiances than the CCR results. The close comparison of these results would indicate that the exponential fit used for the gaseous absorption within the clouds is physically correct. The small differences noted in Figure 3 can be minimized by scaling all subsequent calculated upwelling radiances at the top of the atmosphere by the ratio of the CCR divided by the Rayleigh upwelling radiance. This scaling assumes that the CCR upwelling radiances are perfect, and the differences come from the approximation of the gaseous absorption within the cloud from the exponential fits. Although it does not remove the inaccuracies of the exponential fits, the scaling does give a common base of comparison (CCR upwelling radiances) to subsequent calculations.

The second test used to verify the modification of the program to the HIRS channels was accomplished by inserting a very thin cloud at 700 mbar with a thickness of 0.01 km. Transfer calculations involving such a thin cloud were then carried out. Physically, there should be a slight decrease of the upwelling radiance from the thin cloud when it is compared

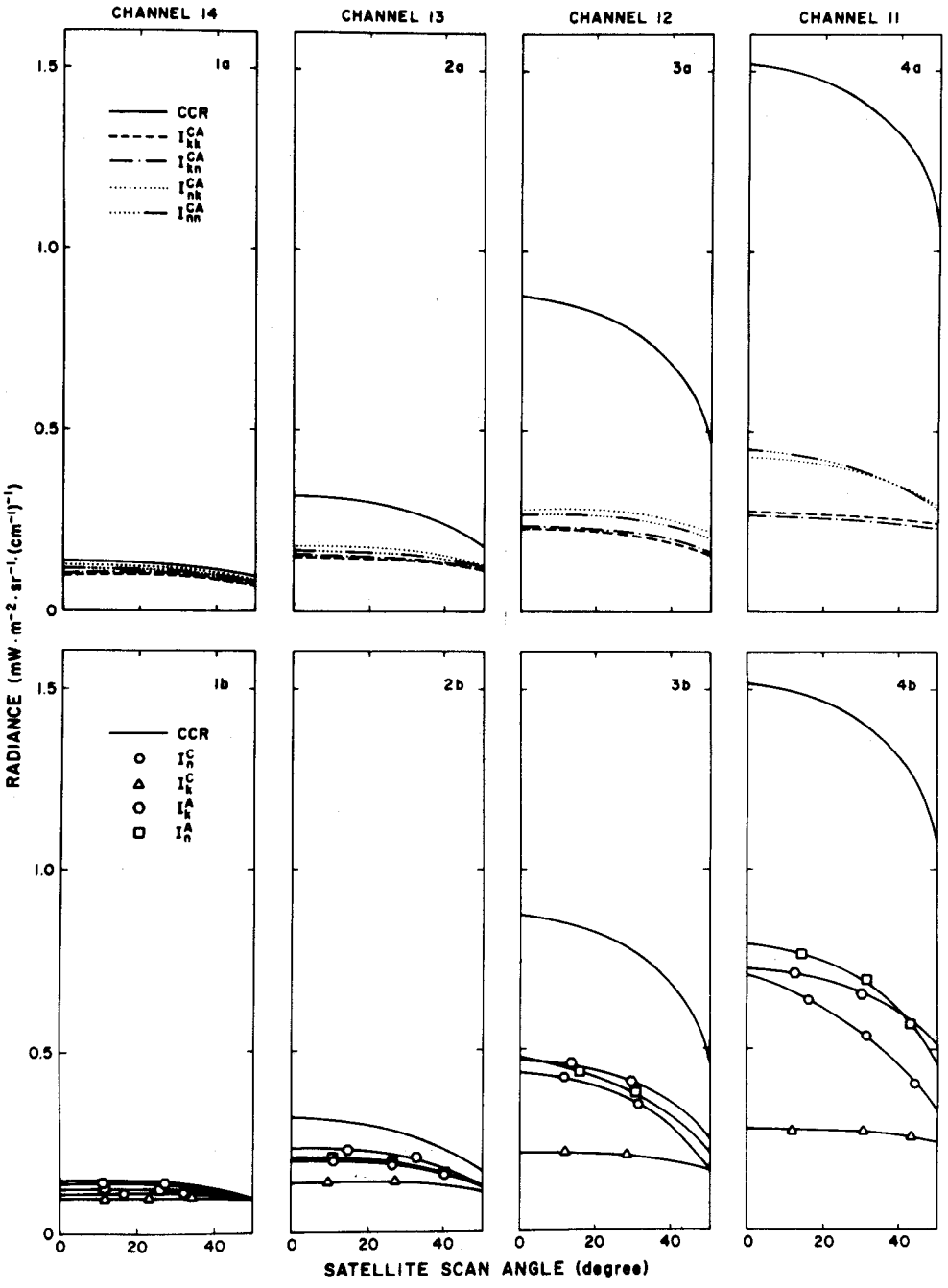

Fig. 5. Comparison of the upwelling radiance for cloudy atmospheres with CCR in shortwave CO_2 channels. The upper panels are for multilayer combinations of thick and thin cirrus and middle cloud. The lower panels are for single layers of thick and thin cirrus and middle cloud.

with the CCR. A plot of the thin cloud case is also shown in Figure 3. It should be noted that in all 12 channels the thin cloud case has less upwelling radiance than the CCR and that the radiance differences between the thin cloud case and CCR are insignificantly small. Although the absolute accuracy of the results is unknown, they do compare well with a similar work done on vertical temperature profile radiometer channels of the NOAA 4 satellite. In order to examine the accuracy of the theoretical results involving clouds, comparisons with satellite-observed cloudy radiances appear necessary. Such comparisons, however, require information on the cloud composition and thickness under the satellite pass so that theoretical transfer calculations may be carried out. Unfortunately, cloud composition information under the satellite pass is normally not available, and it requires a carefully designed field experiment involving aircraft and ground observations.

To actually execute the transfer program, the optical properties for the clouds and the Rayleigh layer (consisting of gases only) become input as well as the atmospheric profile. In section 2 we described the model atmosphere used in this investigation in which the cirrus cloud top and the middle cloud bottom are fixed. It is possible to account for the cloud temperature gradient by dividing the clouds into sublayers. Because of computer storage and computer time limitations, however, only one temperature for cirrus and middle cloud was allowed in the transfer calculations. The cloud temper-

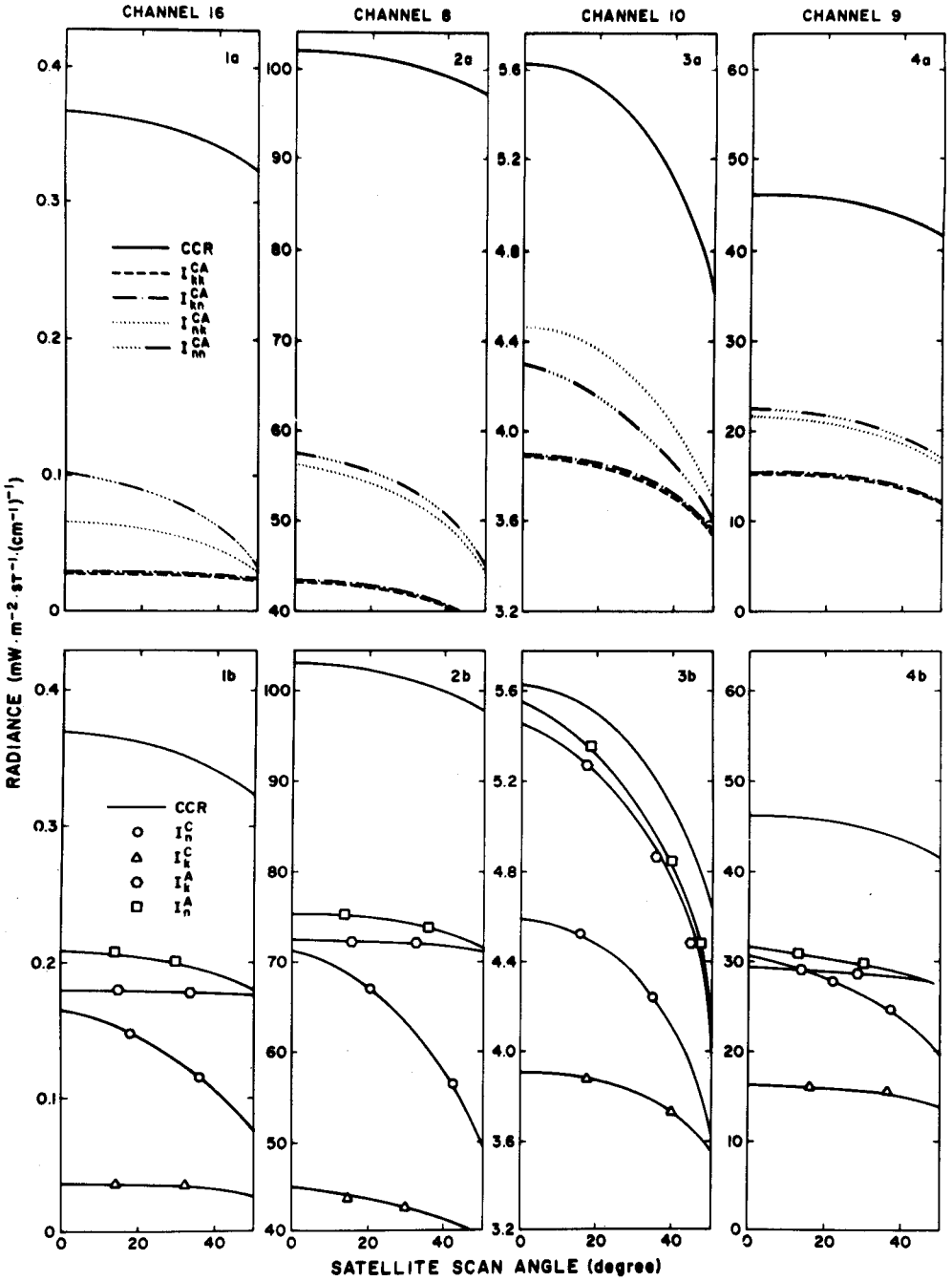

Fig. 6. Comparison of the upwelling radiance for cloudy atmospheres with CCR in window and water vapor channels. The upper panels are for multilayer combinations of thick and thin cirrus and middle cloud. The lower panels are for single layers of thick and thin cirrus and middle cloud.

atures used in all calculations are the averaged temperatures corresponding to the thickest cloud layers obtained from the atmospheric temperature profile. This was necessary to enable us to examine the change in upwelling radiance due strictly to the change in cloud mass by changing the cloud thickness. If more than one parameter was allowed to vary in subsequent calculations, the different temperatures would mask the change in upwelling radiance caused by the change in cloud mass. As will be discussed in section 5, the temperature effect in cloudy radiances may be minimized by dividing the clear column radiance.

The only output from the transfer program utilized in subsequent analysis is the upwelling radiances at the discrete ordinate angles denoted previously coming out of the top of the cloud. These radiance values, which include the radiation contributions from the cloud and the atmosphere below the cloud, are linearly interpolated to 51 angles corresponding to whole satellite scan angles. They are then attenuated to the top of the atmosphere by utilizing the computations described in section 3*d*.

4. Sensitivity Analysis

To conduct sensitivity analysis of the upwelling radiance at the top of the atmosphere, a series of combinations of clouds were inserted into the transfer program. The resulting upwelling radiances at the top of the atmosphere were then

plotted as a function of satellite scan angle. The results of these calculations are shown in Figures 4–6. In each of the cases the lower boundary condition is a summation of the contribution from the ground plus the contribution from each of the atmospheric layers below the cloud.

In each case the top of the cirrus cloud and the base of the altostratus cloud are held constant. To change the cloud combinations, the base of the cirrus cloud and the top of the middle cloud are varied. Since the model atmosphere has ten layers between 700 mbar, the base of the middle cloud, and 250 mbar, the top of the high cloud, the middle cloud could include up to four layers from 700 to 500 mbar, and the high cloud could include up to five layers from 475 to 250 mbar. These ten layers were predetermined from those set in the CCR program. One layer between the two cloud decks must be clear so that three layers exist to insure proper execution of the transfer program. The four symbols used in Figures 4–6 have the following meaning: I_k^C indicates thick cirrus clouds (five atmospheric layers), I_n^C indicates thin cirrus (one atmospheric layer), I_k^A indicates thick middle clouds (four atmospheric layers), and I_n^A indicates thin middle cloud (one atmospheric layer).

The 12 channels of data are divided into the three figures in the following way. Figure 4 contains the four channels in the 15-μm CO_2 band. Plot 1a is for combinations of both high and middle cloud, and plot 1b is for middle or high cloud alone. The same pattern is followed for each set of plots in Figure 4. The plots are arranged from right to left to correspond to decreasing absorption by CO_2. The arrangement of Figure 5 is identical to that of Figure 4 for the four channels in the 4.3-μm CO_2 band. Figure 6 is similar to the previous figures, plots 3 and 4 corresponding to the water vapor bands (channels 10 and 9, respectively). Plots 1 and 2 of Figure 6 correspond to window channels (16 and 8, respectively).

Before discussing the curves in Figures 4, 5, and 6, two additional points must be expanded and must be considered when the results of the figures are interpreted. They are the characteristics of the weighting function and the location in the atmosphere where the satellite receives a maximum of energy for any given channel and the temperature used in the clouds in the transfer calculation.

The sensitivity of upwelling radiance in the presence of clouds is affected by the cloud mass and its temperature. In this model the top of the cirrus cloud remained constant, while the base of the cloud was varied to obtain different thicknesses. By increasing the cloud thickness the upwelling radiance would decrease owing to the cloud mass. At the same time, however, the temperature of the cloud would increase and in effect would increase the upwelling radiance. As a result of these opposite effects from the cloud mass and the temperature in certain occasions the model was indicating greater upwelling radiance from thick cirrus clouds. In order to examine the effects of only cloud mass the temperatures of the cirrus, the Rayleigh, and the middle cloud layers were held constant. In the case of the middle cloud, by increasing the thickness with a fixed base the temperature would decrease, and the two effects would compliment each other. In the figures, I_k^C and I_n^C represent cirrus thicknesses of 4.12 and 1.26 km, respectively. The temperature for the cirrus cloud was taken to be the temperature of I_k^C from the model atmosphere and has a value of 244.9°K. The temperature of the Rayleigh layer was constant in all transfer calculations and was represented by the temperature of the middle layer when both thick cirrus and thick altostratus were present and has a value of 250.1°K. In the figures, I_k^A and I_n^A represent middle cloud thicknesses of 2.68 and 0.35 km, respectively. The middle cloud temperature was that of a thick cloud from the model atmosphere and is represented by a value of 270.17°K. The symbols I_{kk}^{CA} and I_{kn}^{CA} represent multilayered combinations for thick cirrus with thick middle cloud and thick cirrus with thin middle cloud, respectively. I_{nk}^{CA} represents thin cirrus with thick middle cloud, and I_{nn}^{CA} is thin cirrus with thin middle cloud.

The characteristic of the weighting function and the level in the atmosphere where the most energy for a channel is present must be considered in the interpretation of the figures. If the maximum energy of a channel is located above the top of the cloud being examined, the upwelling radiance in the channel will be reduced from the cloud effects in addition to the gaseous absorption above the cloud.

Plots 1a and 1b of Figure 4 are for channel 4 of the HIRS instrument, which is located at 701.91 cm^{-1} in the 15-μm CO_2 band. The weighting function for this channel peaks at 300 mbar. Plots 2a and 2b are for channel 5, located at 716.83 cm^{-1}, and it has its maximum energy from 500 mbar. Channel 6, located at 732.55 cm^{-1} with a maximum energy obtained near 720 mbar, is shown in plots 3a and 3b. The final plot of Figure 4 is for channel 7, which has a central wave number and maximum energy at 749.18 cm^{-1} and 920 mbar, respectively.

Examination of the upper panels of Figure 4 indicates the same general pattern with all four multicloud combinations. The greatest upwelling radiance is obtained from thin cirrus with thick middle cloud in all channels. Although the effects of attenuation above the middle cloud are highly masked by the cirrus cloud, the thin cirrus with thick middle cloud still has the greatest upwelling radiance. In the case of thick cirrus in the upper panels the change of middle cloud thickness has no effect on the upwelling radiance. In the presence of thick cirrus the transfer process is completely dominated by this thick cloud.

The lower panels of Figure 4 display the same general pattern as the upper panels. Single-layer clouds show a greater variability in upwelling radiances. In all cases the thick middle cloud produces the greatest upwelling radiance as discussed earlier. The least radiation comes from the thick cirrus cloud. The larger reduction in the upwelling radiance for cirrus cases is in part due to the colder cirrus temperatures. The cirrus cases show the largest reduction in the upwelling radiance owing to the thickness increase for channel 7, whose peak of the weighting function is near the ground. As the peak of the weighting function moves aloft, effects of cirrus become gradually insignificant, as is evident in channel 4. This is owing to the fact that most of the energy arises from the atmosphere above the cloud. For middle cloud cases, because of the overlapping between the cloud and the peak of the weighting function for channel 7, cloud thickness effects appear to be similar to channels 5 and 6. The decrease in slope of the curves as a function of scan angle for thick cloud cases is consistent with the fact that scattering becomes more isotropic as the cloud thickness increases.

The channels represented in Figure 5 are 14, 13, 12, and 11, which have central wave numbers at 2274.6, 2244.2, 2211.97, and 2191.0 cm^{-1}, respectively. They are located in the 4.3-μm CO_2 band and have their weighting functions peak at 600, 700, 850, and 950 mbar. Figure 5 displays the same characteristics as Figure 3. This would be expected, since they both have CO_2 as the major absorber. In the upper panels of Figure 5 the presence of cirrus cloud again is dominant. There is only a slight change in the upwelling radiance when middle cloud

thicknesses are changed with thin cirrus. Plot 4a of Figure 5 shows an interesting crossing pattern for thin cirrus. This is caused by the location of the level of maximum energy for the channel (950 mbar). In all cases so far discussed, cirrus cloud is the dominant influence. In cases where channels peak higher than the middle base, the thick middle cloud has a greater upwelling radiance than the thin middle cloud.

Since the temperature is held constant, three factors are important in the results of Figure 5. They include the cirrus cloud thickness, the middle cloud thickness, and the peak of the weighting function. In the case of Figure 5, where the crossing pattern is observed, the thickness of the middle cloud has become more dominant than the attenuation above the middle cloud. This factor is useful in using the HIRS data to infer cloud parameters.

Figure 6 is a plot of two HIRS window channels and two water vapor channels. Plots 1 and 2 represent window channels 16 and 8, which have central wave numbers at 2691.2 and 899.99 cm^{-1}, respectively. Since these are window channels, they receive the maximum energy from the earth's surface. Plots 1a and 2a show the results in the presence of multilayered clouds. With the absence of major absorbing gases in the atmosphere the problems cited in the CO_2 channels concerning absorption above the cloud are now minimal. This can be seen by noting the greater difference between thick and thin middle cloud in the presence of thin cirrus when compared with Figures 4 and 5. Plots 1b and 2b of Figure 6 also indicate the effects of clouds on upwelling radiance more readily than the CO_2 channels. As would be expected, thin clouds have a greater upwelling radiance than thick clouds. Cirrus clouds attenuate more radiation than middle clouds when only one cloud deck is present. This last point can be attributed in part to the temperature of the two clouds.

Plots 3 and 4 of Figure 6 correspond to channels 10 and 9, respectively. Channel 10 peaks at 400 mbar and has a central wave number of 1508.29 cm^{-1}. Channel 9 peaks at 900 mbar and has a central wave number of 1223.22 cm^{-1}. Since the concentration of CO_2 in the atmosphere is independent of temperature, the crossing patterns observed in Figures 4 and 5 will always be present. On the other hand, however, the concentration of water vapor is a function of temperature, and the gaseous absorption above the cloud will vary with temperature in channel 10. The gaseous absorption in the clouds was fitted with the saturation conditions as noted earlier. In the case of the Rayleigh layer the prevailing moisture concentration of the model atmosphere was assumed. The crossing pattern for thick and thin middle clouds is not present for the water vapor channels. This can be attributed to the fact that the thickness of the middle cloud has a greater effect on the final upwelling radiance than the absorption above the cloud, although the real effects of the middle cloud are somewhat less owing to the gaseous absorption above the cloud. The same patterns are observed in the water vapor channels as in all other channels analyzed. The thick cirrus cloud dominates in plots 3a and 4a and has the same upwelling radiance for thick cirrus in 3b and 4b of Figure 6.

5. A Case Study on the Cloud Thickness Estimation

As was noted earlier, the theoretical model calculated upwelling radiances for one atmosphere, one cloud temperature, one cloud composition, and over the scan angles of the HIRS instrument. In addition, the cloud top height for the cirrus and the cloud base for the middle cloud were held constant. In the real atmosphere the temperature profile is always changing, the cloud composition is variable, and the location of the clouds in the vertical is never constant. A method that will minimize the effects of the model assumptions is desirable.

To minimize the model assumptions and to normalize the real data to the model, the clear column radiances were divided into the cloudy radiances for each channel. This ratio represents the relative reduction of upwelling radiances due to the cloud effects in the atmosphere, and the quantity is dimensionless. There are several advantages in working with these ratios. Physically, the ratio will reduce the effect of the change in atmospheric profile on the cloudy radiances. In addition, the degradation of the ratio coupled with the peaking of the weighting function gives an immediate indication of clouds at that level or above. Another advantage of the ratio technique is that in addition to normalization between different atmospheres, the effects of clouds on the ratio of each channel can be compared with those of other channels. In the subsequent analysis, channels 4–7 of the 15-μm CO_2 band, channels 11–14 of the 4.3-μm CO_2 band, channel 8 at 11.1 μm in the window, channel 9 in the 8.2-μm water vapor band, and channel 10 in the 6.3-μm water vapor band were utilized.

The theoretical model was executed for cirrus thicknesses of 1, 2, 3, and 4 km for the case study described below. These ratios are plotted in Figure 7 (solid lines). Examination of Figure 7 shows that the transparent quality of cirrus is evident in the infrared spectrum. There is a successive decrease of upwelling radiances in all channels as the cloud thicknesses increase. The successive decrease of the ratios continues all the way to 4 km. Between 3 and 4 km the decrease in the ratio in each channel is only slight, a feature indicating that near 4 km the cirrus cloud used in the model is becoming opaque to the infrared radiation.

Intercomparisons of the channels in Figure 7 give a good indication of the effects of clouds on upwelling radiances for different wave number regions of the infrared spectrum in conjunction with the peak of the channels' weighting functions. The physical factors that influence the ratio for a given cloud type, cloud thickness, and channel could be determined from ratios presented in Figure 7. In the present model the cloud top is constant at 250 mbar. By using a 2-km cirrus as an example the interaction of these two physical factors (the weighting function and the channel wave number) is examined. The channels that are in the 15-μm CO_2 band show a decreasing ratio as the weighting functions peak deeper in the atmosphere. The same decrease is noted in the 4.3-μm CO_2 channels but by a greater degree. This fact would indicate a greater impact of clouds on shorter wavelengths. The result shows this effect when channel 7 (peak at 900 mbar) and channel 12 (peak at 850 mbar) are compared, where the longwave channel has a ratio double that of the shortwave channel.

The HIRS data set chosen for the case study was from the data set obtained for August 20–30, 1975, a time when all channels of the HIRS instrument were operating properly. A total of 26 passes were available in the data set of which one (August 25) was analyzed for cloud information at scan angles closest to nadir.

Inspection of NOAA satellite pictures on this day (Figure 8) shows cirrus shield associated with a squall line near 40°N. The points used in the cloud thickness estimates are from this general area. The NOAA 4 satellite data for the day are the mapped, normalized, and gridded mosaics from the very high

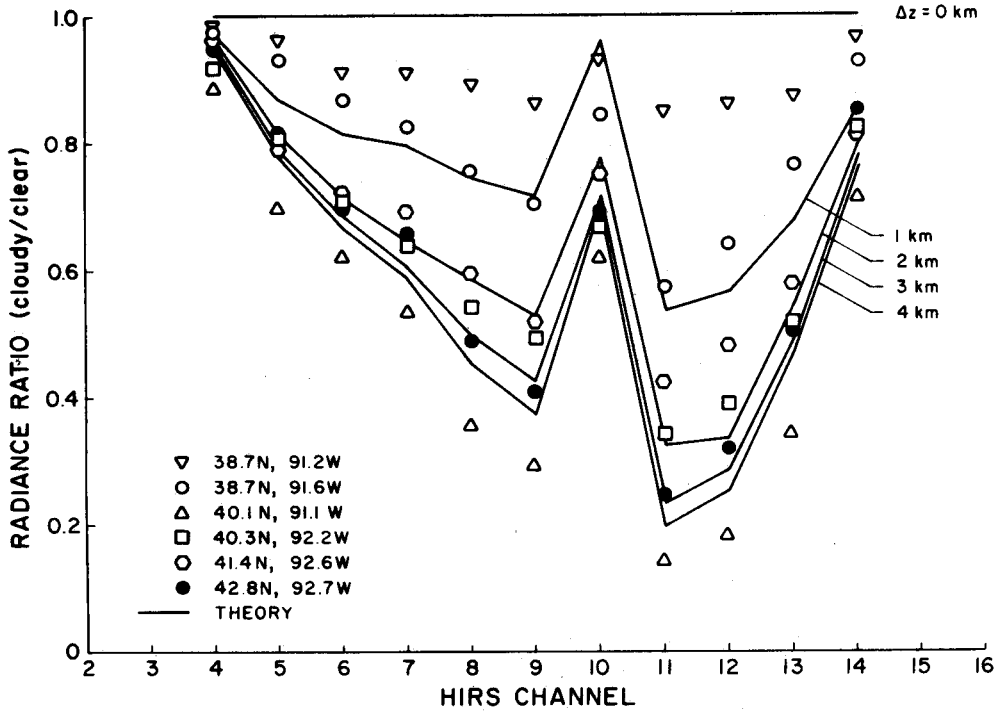

Fig. 7. Comparison of theoretical results (solid curves) and satellite HIRS data (inverted triangles, open circles, triangles, squares, hexagons, and solid circles) for the 11 HIRS channels in terms of the cloudy to clear column radiance ratios.

resolution radiometer. A two-picture set shown in Figure 8 includes the broadband visible channel from 0.5 to 0.7 μm and the broadband window channel from 10.5 to 12.5 μm.

To apply the theoretical results to the real HIRS data, a method had to be developed to reduce the cloudy radiances to ratios. The theoretical data would be compatible, since the atmospheres used in the calculations were mid-latitude summer and the real data are also for mid-latitude summer. To obtain a clear column radiance that is representative of a localized area, the HIRS data were examined in conjunction with the satellite pictures. The point chosen for the clear column radiance (at about 38°N, 91°W) was then used to obtain the cloudy ratios for that day. The point chosen has the same scan angle as the cloudy radiances.

In reference to Figure 8 we have selected a number of locations at about 40°N and 90°W along the satellite track for the inference of cloud thickness based on the theoretical sensitivity analyses described previously. Examinations of these cloud photographs as well as of synoptic surface and 500-mbar maps show that the cloud is cirrus with no low cloud present below. Six scan radiance ratios are depicted in Figure 7. The scan points at 38.7°N, 91.2°W (inverted triangles) and 38.7°N, 91.6°W (open circles) represent areas that are close to the cirrus edge. On the basis of comparisons with the theoretical curves, thicknesses of 0.5 and 1 km were estimated. As the satellite scan goes deeper into the cloud center, a thickness of greater than 4 km (40.1°N, 92.1°W (triangles)) is obtained. Other scans further north under investigation indicate cirrus thicknesses of the order of 2–3 km, as illustrated by the square, hexagon, and solid circle. Note that the resolution of HIRS instruments is approximately 23 km at nadir. From this case study it appears that the HIRS radiance ratios resemble reasonably well those calculated from the theoretical analyses. The 4.3- and 15-μm CO_2 channels behave especially well. However, the water vapor channels show some nonsystematic variations, perhaps owing to the use of the observed clear column radiance, which arises from an atmosphere differing from cloudy cases.

6. Conclusions

A theoretical model that calculates transfer of spectral infrared radiation was developed to include cirrus and middle clouds and absorbing gases. This current analysis used one model atmosphere and one middle and high cloud type for all the calculations. The top of the cirrus cloud and the base of the middle cloud were held constant to minimize computer time. The layers in the transfer computations were assumed to have constant temperatures so that the effects of the change in cloud thickness on the upwelling radiance could be studied. Various thicknesses and combinations of middle and cirrus clouds were used in the analysis. This model was then applied to the HIRS channels of the Nimbus 6 satellite. Available transmittances for each of the channels used were employed and modified to generate upper and lower boundary conditions and gaseous absorption in and between the cloud layers.

The model was then used to generate upwelling radiances over a range of satellite scan angles for these combinations of clouds. Comparison of the results shows that the thick cirrus dominates the transfer process. In addition, the thick middle cloud had a greater upwelling radiance at all angles when compared with the thin middle cloud in the 15-μm CO_2 band and in the 4.3-μm CO_2 band channels that have weighting functions above the thin middle cloud top. This reversal of expected results is caused by the attenuation of the upwelling radiance by the gases above the cloud. The results also show that the window channels and water vapor channels do not have this effect for the model atmosphere used.

In the case of multilayered clouds the differences between

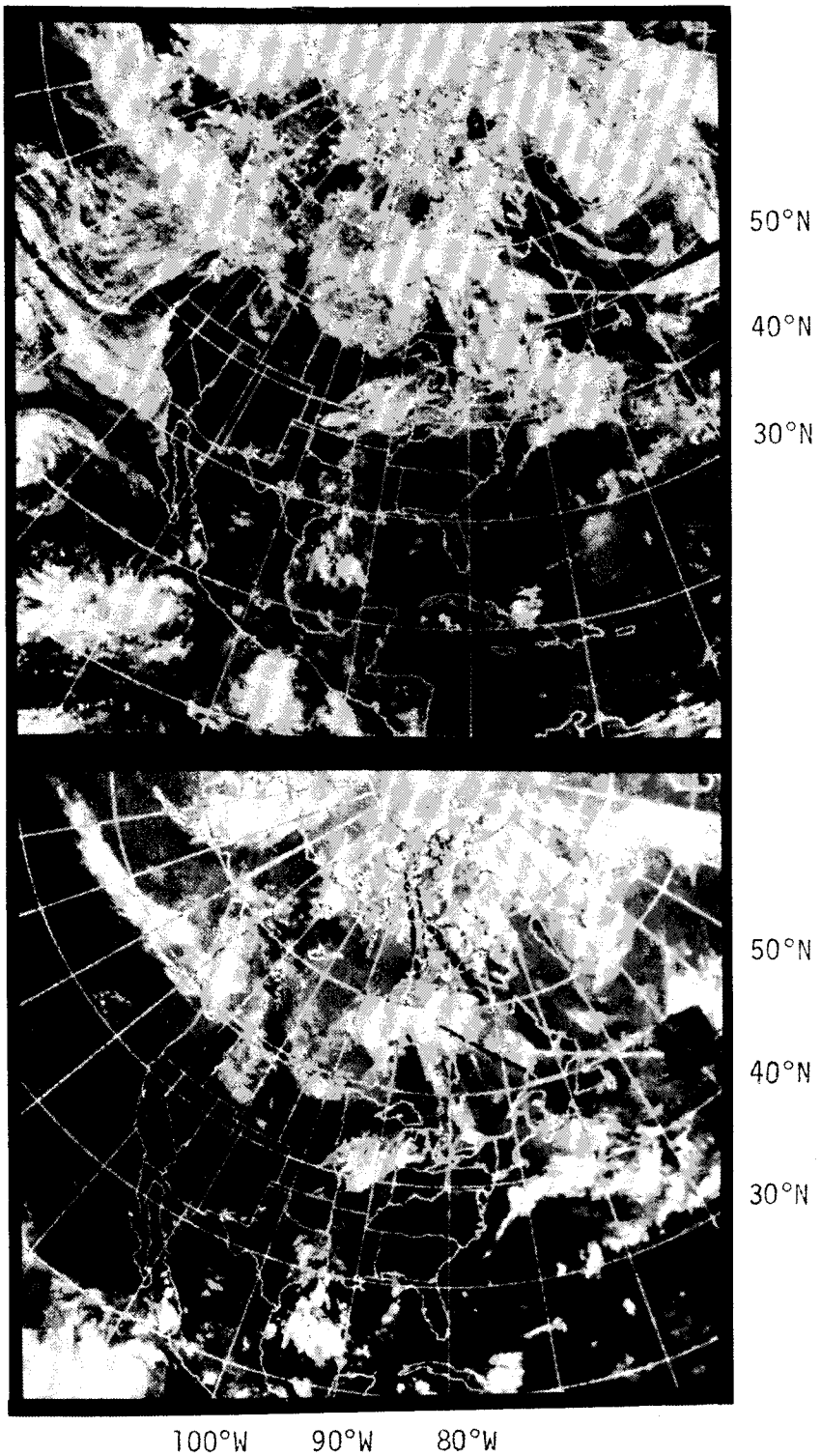

Fig. 8. NOAA 4 mosaic for August 25, 1975, with the visible channel on the top and the infrared channel on the bottom.

the four multicloud combinations are reduced in comparison with the single-layer cases. In the case of thick cirrus, changes in the middle cloud thickness below do not affect the upwelling radiance, since the thick cirrus dominates the transfer processes. For thin cirrus clouds, changing the middle cloud thickness does show a small effect on the final upwelling radiance. The thick middle cloud alone has greater upwelling radiance than the thin middle cloud in all channels that peak above the thin middle cloud top. The shortwave CO_2 channels show a slightly better contrast in the thin cirrus case of multilayered clouds than the longwave CO_2 channels. The window and water vapor channels show a greater contrast than the shortwave CO_2 channels.

On the basis of the theoretical sensitivity analysis a case study using the actual HIRS radiance data has been carried out for the determination of the cirrus cloud thickness. The case study involves the ratios of the cloudy to clear column radiances in which the atmospheric temperature effect is mini-

mized. We show that it is feasible to estimate the cirrus cloud thickness by employing the combination of infrared channels with the assistance of IR and visible cloud pictures from the NOAA 4 satellite. On the basis of this investigation it seems possible to establish empirical relationships between HIRS-type data and certain cloud parameters derived from the theoretical analyses presented in this paper.

Acknowledgments. We are grateful to H. M. Woolf of NESS for providing us with the HIRS transmittance routine. This research was supported by the Air Force Geophysics Laboratory under contract F19628-75-C-0107.

REFERENCES

Bunting, J. R., and J. H. Conover, Estimates from satellites of total ice and water content of clouds, in *Proceedings of the International Conference on Cloud Physics*, pp. 407–412, American Meteorological Society, Boston, Mass., 1976.

Chahine, M. T., Remote sounding of cloudy atmospheres, 1, The single cloud layer, *J. Atmos. Sci.*, *31*, 233–243, 1974.

Chandrasekhar, S., *Radiative Transfer*, 393 pp., Dover, New York, 1950.

Feddes, R. G., and R. D. Smith, A synoptic scale model for simulating condensed atmospheric moisture, *USAFETAC Rep. TN74-4*, 31 pp., U.S. Air Force Environ. Tech. Appl. Center, Washington, D. C., 1974.

Hale, G. M., and M. R. Querry, Optical constants of water in the 200 nm to 200 μm wavelength region, *Appl. Opt.*, *12*, 555–563, 1973.

Houghton, J. T., and G. E. Hunt, The detection of ice clouds from remote measurements of their emission in the far infrared, *Quart. J. Roy. Meteorol. Soc.*, *96*, 1–17, 1971.

Kaveney, W. J., R. G. Feddes, and K.-N. Liou, Statistical inference of cloud thickness from NOAA IV scanning radiometer data, *Mon. Weather Rev.*, *13*, 99–107, 1977.

Liou, K.-N., Light scattering by ice clouds in the visible and infrared: A theoretical study, *J. Atmos. Sci.*, *29*, 524–536, 1972.

Liou, K.-N., A numerical experiment on Chandrasekhar's discrete-ordinate method for radiative transfer: Applications to cloudy and hazy atmospheres, *J. Atmos. Sci.*, *30*, 1303–1326, 1973.

Liou, K.-N., On the radiative properties of cirrus in the window region and their influence on remote sensing of the atmosphere, *J. Atmos. Sci.*, *31*, 522–532, 1974.

Liou, K.-N., Remote sensing of the thickness and composition of cirrus clouds from satellites, *J. Appl. Meteorol.*, *12*, 91–99, 1977.

McClatchey, R. A., et al., Optical properties of the atmosphere, *Environ. Res. Pap. 354*, Air Force Cambridge Res. Lab., Bedford, Mass., 1971.

Miller, D. B., and R. G. Feddes, *Global Atlas of Relative Cloud Cover 1967–1970 Based on Data From Operational Satellites*, 237 pp., National Environmental Satellite Service, Washington, D. C., 1971.

Park, S. U., D. N. Sidkar, and V. E. Suomi, Correlation between cloud thickness and brightness using Nimbus 4 THIR data (11.5 channel) and ATS 3 digital data, *J. Appl. Meteorol.*, *13*, 402–410, 1974.

Schaaf, J. W., and D. Williams, Optical constants of ice in the infrared, *J. Opt. Soc. Amer.*, *63*, 726–732, 1973.

Smith, W. L., and H. M. Woolf, The use of eigenvectors of statistical covariance matrices for interpreting satellite sounding radiometer observations, *J. Atmos, Sci.*, *33*, 1127–1140, 1976.

Smith, W. L., P. G. Abel, H. M. Woolf, A. W. McCulloch, and B. J. Johnson, The high resolution infrared radiation sounder (HIRS) experiment, in *Nimbus VI Users Guide*, 227 pp., NASA Goddard Space Flight Center, Greenbelt, Md., 1975.

Taylor, F. W., Remote temperature sounding in the presence of cloud by zenith scanning, *Appl. Opt.*, *13*, 1559–1566, 1974.

(Received January 31, 1977;
revised July 26, 1977;
accepted July 28, 1977.)